8-2007

Experimental analysis of plasma conditions in an inverted cylindrical magnetron sputtering system

Bradley Handloser
University of Arkansas, Fayetteville

Experimental Analysis of Plasma Conditions in an Inverted Cylindrical Magnetron Sputtering System

Honors Thesis submitted in Partial Fulfillment of the
Requirements for the Honors Program for the
Degree of Bachelor of Science
In Mechanical Engineering

2007

Bradley Scott Handloser

Project Advisor – Dr. Matt Gordon

Mechanical Engineering
University of Arkansas, Fayetteville

Table of Contents

List of Tables

List of Figures

Chapter One

1.0 Abstract

In this report, we will investigate Langmuir probe and mass spectrometer plasma diagnostic systems used to characterize conditions within a magnetron sputtering system. The specific systems used were the ESP*ION* Langmuir probe and EQP mass spectrometer by Hiden Analytical and the ICM-10 inverted cylindrical magnetron sputtering system by Isoflux, Inc. This paper will show how these systems work, are operated, and produce data. Low power oxygen and argon plasmas were used through this research for diagnostics. With the EQP, two modes were used to collect data: RGA for neutrals and radicals and SIMS for positive ions. With both modes, mass and energy scans were produced. With the ESP*ION*, current vs. voltage (I-V), first differential, second differential, and electron energy distribution functions (EEDF) were created. Also I-V curves at different locations within our sputtering system were made and compared. This preliminary research will help to lay the ground work for others to produce a true characterization of our system and so that in the future correlations can be made between the plasma conditions present and the quality of the films deposited.

1.1 Introduction

Magnetron sputtering has become a widely used technique for the deposition of high quality thin films and coatings. Some common applications include thin film solar cells, magnetic recording media, metallic interconnects, high wear resistive coatings, Aluminum coatings and functional glass coatings [1]. The process can deposit a wide variety of materials including metals, metal alloys, nitrides, carbides and oxides can be

deposited [13]. One reason for the success of magnetron sputtering is its unique ability to retain specific design requirements in a cost-effective manner. Another reason magnetron sputtering is among the most widely used physical vapor deposition (PVD) processes is because it is seen as environmentally friendly due to the fact that it avoids using harsh chemical reactants [5].

Typically, magnetron sputtering sources are operated between a frequency of 10 to 350 kHz and a duty cycle from 50% to 90%. A low pressure, around 0.5 Pa or lower, is also an essential part of the process [11]. In order for the sputtering to occur within the system, a plasma, or partially ionized gas, must be created. This is done by charging the low-pressure gas with an electrical field which causes the gaseous particles to lose an electron or become ionized. These plasmas consist of various neutral atoms, ions, radicals, and free electrons. The positively charged ions, along with energetic neutrals, are then accelerated via a strong magnetic field into the target consisting of a desired material. When these highly energized particles collide with the target, atoms are ejected or sputtered from its surface. These sputtered particles, consisting of a specific material, eventually condense and react with the substrate to become a thin film layer [4]. The external parameters of the sputtering system including frequency, power, pressure, system configuration, gas or gases used, and target material govern the characteristics of the plasma and ultimately the films created. In order to analyze the plasmas being created, diagnostics tools such as Langmuir probes and mass spectrometers are used.

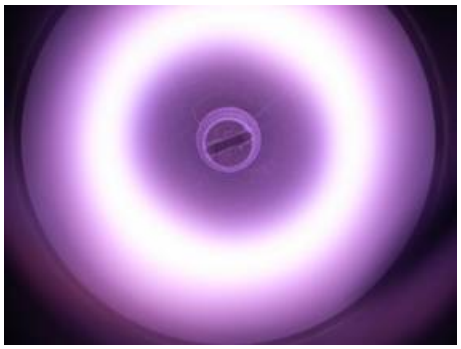

Figure 1: Plasma created in cylindrical magnetron [10]

In this thesis, ways by which the magnetron plasma would be characterized by our research group is considered and a set of preliminary data has been reported here to illustrate what set of parameters can be investigated. Though the data reported here is not ideal, they were not taken at deposition conditions due to temperature issues, it gives the group a fair understanding of what to expert at high powers.

Chapter Two

2.0 Physical Vapor Deposition

Physical vapor deposition (PVD) is a process that produces a certain atomic, molecular, or ionic species that are transported and condensed on a substrate. The three fundamental PVD processes include sputtering, evaporating, and ion plating. The evaporation process requires that a material be vaporized by thermal heat at an adequately low pressure. The vapor then can move freely and condense on the substrate. Sputtering occurs when a solid surface is bombarded by highly energized particle causing surface atoms to be knocked free. Ion plating uses aspects of both the evaporation and sputtering processes [12].

2.1 Magnetron Sputtering System

This is a fine technique of depositing thin-films onto substrates. Unlike evaporation, the materials to be sputtered do not have to be heated. The material is in the form of a thin plate called a target. The target is mounted in a chamber filled with Argon gas at low pressure. Positive argon ions are produced in the plasma (formed when the target is

connected to negative high voltage) by collisions of electrons with argon atoms that are accelerated toward the negatively-charged target. Upon impact with the target, free atoms of the target material are expelled and deposited on substrates mounted in front of the target, building a thin-film. Unlike ordinary sputtering processes, all the ions that attempt to escape the target, are captured behind/at the sides of the targets and are confined to the immediate vicinity of the target by strong permanent magnets. This increases the ion current resulting in a fast deposition. The target temperature is low thus resulting in a high quality film deposited.

2.2 The Inverted Cylindrical Magnetron System

The three major sputtering deposition techniques are DC (diode), RF (radio frequency), and AC (alternating current). The sputtering system used for our experiments, the ICM-10 made by Isoflux Inc., is an inverted cylindrical magnetron sputtering system that uses an AC power supply [12]. The system is made of two hollow cylindrical targets that completely surround the substrate. This configuration is advantageous over planar magnetrons because it has the ability to coat complex 3-D shapes. The system also implements a patented unbalanced magnetic field. Each target has a set of magnetic poles that is stronger than the other causing the magnetic field lines to focus towards the center. The unbalanced magnetic field produces extremely high plasma densities, much higher than conventional DC sputtering systems. The ICM-10's AC power supply enables its electrically isolated targets to each switch back and forth between being a cathode and anode. This allows the system to naturally produce high deposition rates without damaging arcing. In most other configurations, complex wiring in needed to

avoid this problem. The system is also capable of producing current densities much higher than other systems at similar target power and bias voltages (Glocker ICM10 paper).

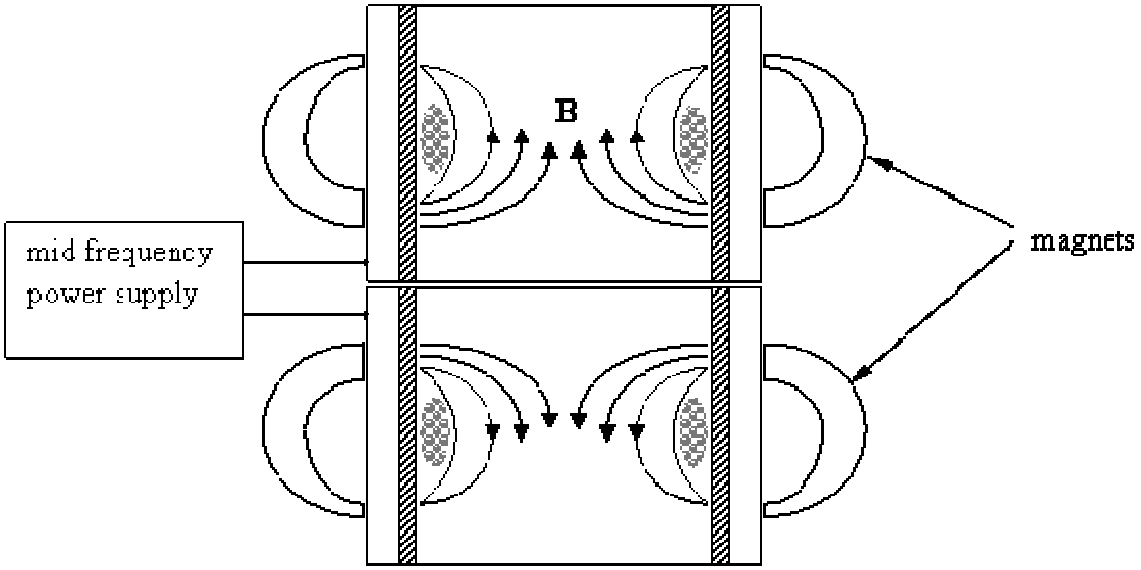

Figure 2: Diagram of magnetic fields in inverted cylindrical magnetron system using AC power [6]

Our specific system uses three targets approximately 33 cm in diameter and 7.5 cm tall. The three targets are stacked on top of one another with small spacers separating each of them. The middle of the three targets is dead or inactive and also acts as a spacer. Like most systems, it operates at an extremely low pressure (2mTorr) which is essential for plasma production. The system is operated on a PLC platform and RSView 32 HMI interface. The system uses the PEII AC power supply made by Advanced Energy. This power supply operates at 41 kHz and has a maximum power of 10 kW. The DC bias power supply to the substrate can also reach a maximum of 5 kW. Argon, Oxygen, and Nitrogen are the main gases used in the ICM system. Ar is always used first to ignite the

plasma before the other gases are introduced. The two active targets are made of aluminum and the walls are water-cooled to control temperature.

One of the primary goals for our ICM-10 system is to deposit α-alumina thin films on steel and industrial tools. This is a highly sought after goal in the field of Surface Engineering because of the outstanding properties of aluminum oxide films in metal cutting. . The conventional alumina deposition process requires a substrate temperature of 750-1000ºC which is harmful to temperature-sensitive steels (degrade at 500-700 ºC). Low temperature (≤ 500ºC) α-alumina deposition has proven to be difficult; however, preliminary data from the inverted cylindrical magnetron sputtering system indicate possible success.

Chapter Three

3.0 Experiments

In this section, the alumina thin film growth process, new plate designs and the plasma diagnostics data acquisition process with the state-of-the-art tools: Langmuir probe and EQP are mentioned briefly.

Figure 3: Experimental sputtering system, ICM-10 made by Isoflux

3.1 The Deposition Process

The ICM system is computer controlled by using a spreadsheet-like program to run the system. The required parameters for any growth process are entered into the spreadsheet (table 1). All parameters listed in table one can be altered within the limits of the equipment. These parameters eventually determine the quality of the material deposited, thus careful adjustments will result in quality films. For instance below is of the recipe one of the recipes used in the attempted creation of α-alumina plasma.

Table 1: Plasma recipe for alpha-alumina growth

	Step 1	Step 2	Step 3	Step 4
Argon (0 - 200 sccm)	150	150	80	45
Oxygen (0 - 200 sccm)	0	0	0	45
MDX Mode (I/V/P)	P	V	V	V
MDX (I = 0-10, V = 0-1000, P = 0-5000)	100	200	50	35
PE II Mode (I/V/P)	P	P	P	P
PE II (I = 0-35, V = 0-1100, P = 0-10000)	500	1000	5000	5000
Shutter (Open/Closed)	Closed	Closed	Closed	Open
Step Time (Seconds)	60	300	300	7200

	Step 5	Step 6	Step 7	Step 8
Argon (0 - 200 sccm)	150	45	150	45
Oxygen (0 - 200 sccm)	0	45	0	45
MDX Mode (I/V/P)	V	V	V	V
MDX (I = 0-10, V = 0-1000, P = 0-5000)	0	35	0	35
PE II Mode (I/V/P)	P	P	P	P
PE II (I = 0-35, V = 0-1100, P = 0-10000)	5000	5000	5000	5000
Shutter (Open/Closed)	Closed	Open	Closed	Open
Step Time (Seconds)	300	7200	300	7200

The primary function of steps 1 and 2 are to ignite the plasma. Only Ar gas is present in this step and the shutter to the target is closed. The shutter is a circular wall that prohibits any sputtered particles from getting to the target for deposition. The MDX, which is the bias on the substrate, is also warming up. In step 3, there is still no sputtering but a significant increase in power is initiated to warm up the power supply. Step 4 marks the beginning of sputtering and deposition. The power is sufficiently high at 5000V, Ar and O_2 are now present, the shutter to the targets is open, and the time is increased to 7200s. This deposition step is then followed by a cleaning step. The shutter is now closed and there is no bias on the substrate to stop deposition. Again only Argon plasma is present which continues the sputtering process; this essentially cleans the Aluminum targets. Steps 4 and 5 are then repeated until the desired thickness of the film is achieved.

3.2 Mass Spectrometer

Mass spectrometers are used in plasma diagnostics to measure characteristics of individual molecules present in a system. Their analysis includes a combined Mass/Energy measurement for positive and negative ions, neutrals, and radicals [3]. Neutrals and radicals must be ionized before sampling while the positive and negative ions are directly sampled. All of the species must be charged so they can be moved and

filtered by external electric and magnetic fields for sampling [12]. With this data, an energy resolved mass spectra of the molecules present and created within the plasma can be produced.

The mass spectrometer used for plasma diagnostics in our experiments was the HAL Electostatic Quadrupole Plasma (EQP) Analyser built by Hiden Analytical Limited. The EQP is a "high-transmission 45˚ sector field ion energy analyzer and quadrupole mass spectrometer" [3]. It measures the energy and mass-to-charge ratio distributions of positive and negative ions, neutrals, and radicals generated in the source plasma. The EQP system contains ion extractor optics, ioniser, sector field energy analyser, triple filter mass analyser, pulse ion counting detector, and MASsoft PC data system for control and analysis (EQP/EQS Analyser Operator's Manual, 1-5).

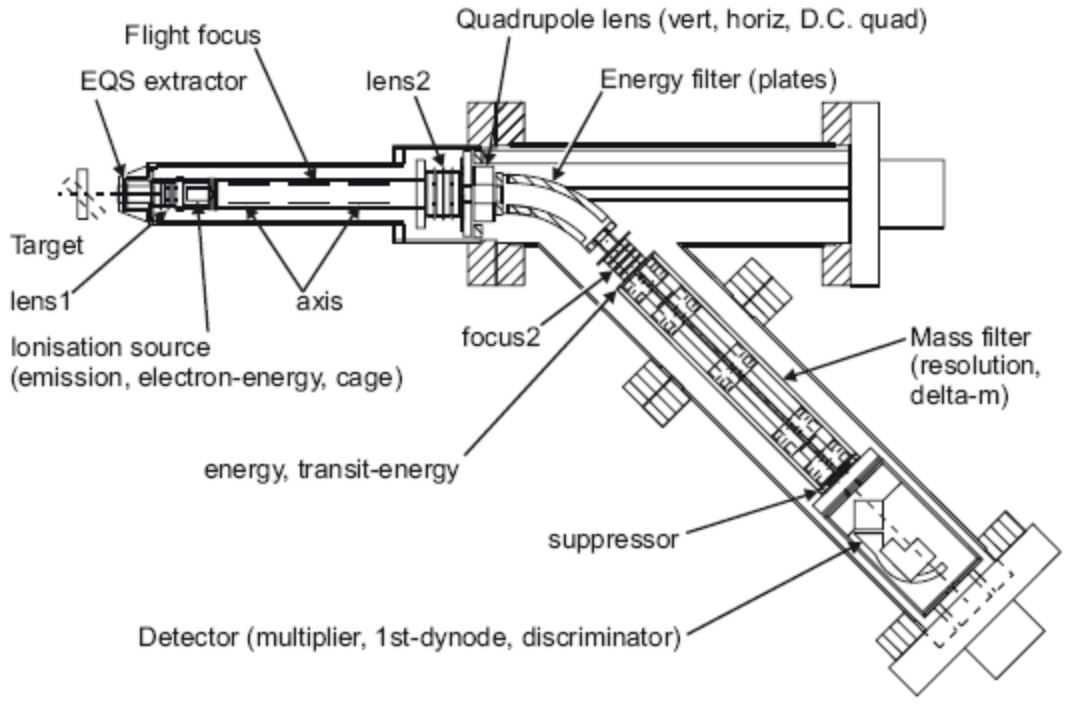

Figure 4: Schematic of EQP system by Hiden Analytical, Inc. [3]

There are two modes of analysis available with the EPQ system: Secondary Ion Mass Spectrometry (SIMS) and Residual Gas Analysis (RGA). The SIMS mode analyzes the mass and energy of ions generated in the plasma while the RGA mode analyzes the mass and energy of neutrals and radicals. Positive and negative ions can be simply extracted by the EQP system because they already possess a charge. For RGA, the neutrals and radicals must be ionized by the ionization source located closely behind the extractor opening. Ionization is achieved by electron impact (EI) via thermionic emission from a hot filament. Molecules are normally converted to positively charged particles in this process [10].

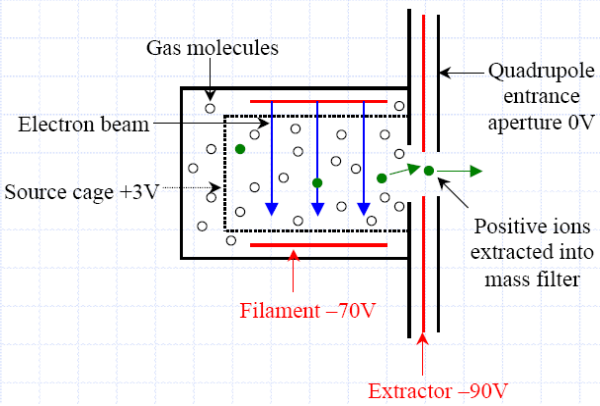

Figure 5: Electron impact ionisation by hot filament [10]

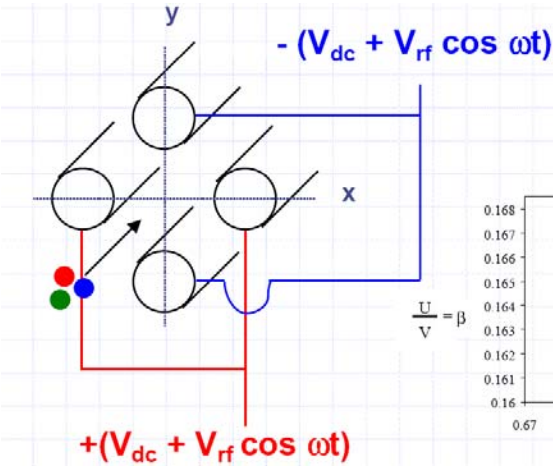

Figure 6: Quadrupole mass filter, z-axis propagation [10]

All ions, both SIMS and RGA mode, are then focused into an electrostatic energy field analyser, a triple-section quadrupole mass filter, and finally a detector [3]. The electro static energy field analyser is a 45˚ sector field which measures the curves of ions to determine their kinetic energies [1]. The triple-section quadrupole is a mass filter that differentiates ions present and produced for detection. The quadrupole is comprised

of two pairs of parallel metal rods of equal length. They contain fixed direct current (DC) and alternating radio frequency (RF) components [10]. One pair consist of a DC component (V_{DC}) at an opposite potential compared to the other, while the other pair has an RF (V_{RF} cos ωt) component 180˚ out of phase of its adjacent rod [1]. All ions entering the quadrupole are deflected from their original trajectory and those without the exact mass : charge (m/e) ratio desired are deflected and neutralized upon impact on the rods. The change in RF enables only one certain m/e ratio at a time to oscillate down the z-axis.

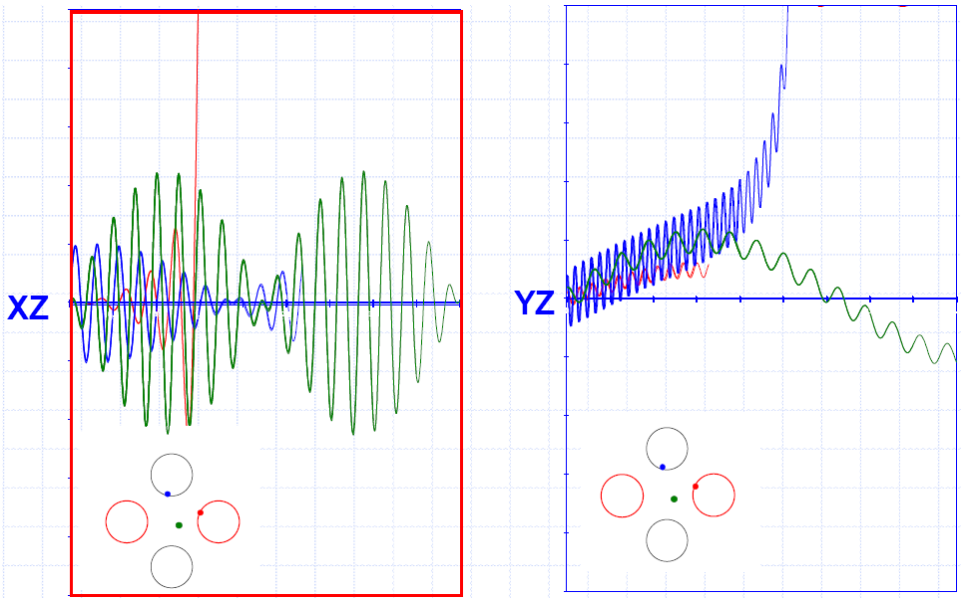

Figure 7: Qaudrupole mass filter Mathieu Stability Diagrams [10]

The desired ions that make it through produce an ion current on the detector. The detector used by the EQP is a secondary electron multiplier (SEM). When an ion impacts the surface of the SEM, 2 or 3 electrons are generated. These electrons are further multiplied in a cascade affect, via an applied voltage, when they collide with the surface. The multiplier effect normally produces a magnitude of 10^3 greater than the actual count

[10]. The output from the detector is given in arbitrary units of 'counts per second.' This output is normally paired in a graph versus either mass or energy because the m/e ratio of the desired ion is known [1].

3.3 Langmuir Probe

The Langmuir Probe diagnostic tool was first developed by Mott-Smith and Langmuir in 1926 [1].

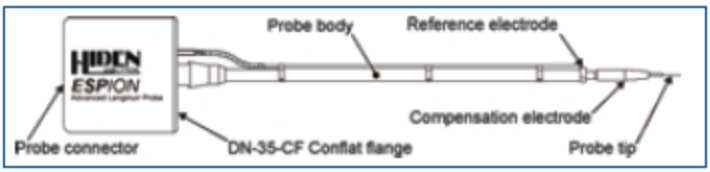

Figure 8: Schematic of ESPION Langmuir probe made by Hiden Analytical, Inc. [7]

The probe is a small electrode consisting of a conductive material that is connected in series to a variable voltage source. This source is necessary to bias the probe positively or negatively against the plasma. When placed in the plasma, the electrons and ions present produce a current in the probe. The current drawn from the plasma is then measured as a function of the bias voltage. This is known as the current-voltage (I-V) characteristic [13]. From the I-V curve, several basic plasma properties can be obtained including ion density (n_i), electron density (n_e), electron temperature distribution (T_e), plasma potential (V_p), and electron energy distribution function (EEDF) [7].

The plasma potential (V_p) is the curve located between the two lines in the upper right region (knee) of the I-V curve. At this location, the probe potential (V_B) is equal to the plasma potential. Mostly electron current is collected here due to the fact that electrons are considerably lighter and more mobile than other species (i.e. ions, neutral, and radical). The region to the right of the plasma potential with the slightly positive slope is known as the electron saturation region.

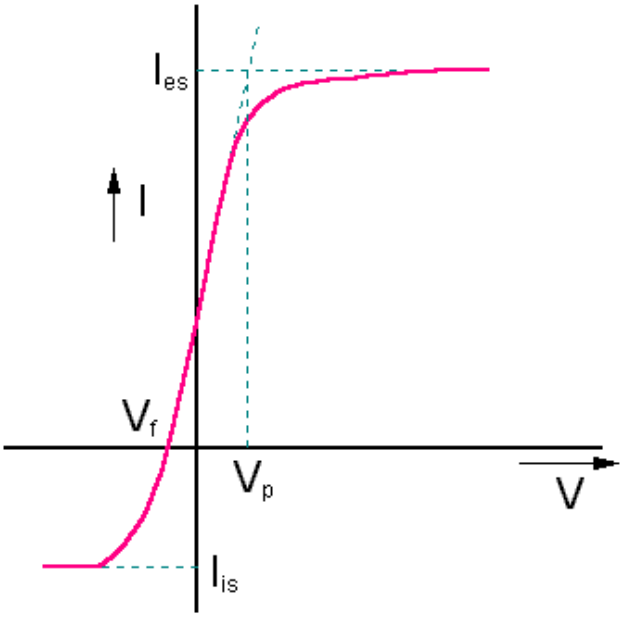

Figure 9: Typical I-V curve generated by Langmuir probe [7]

The Langmuir probe used in our experiments was the ESP*ION* made by Hiden Analytical, Inc. It can measure ion (n_i) and electron density (n_e) over the range of 10^{14} to 10^{19} m^{-3} and electron temperature (T_e) up to 10 eV. It has a voltage range of -200V to 100V and a current range of 20μA to 1A. Our system has the optional automatic z – translator capable of taking measurement over 300mm in the z-direction. The probe is RF compensated and is designed for high frequency plasma. Our probe tip is made out of titanium rather than the standard tungsten to stop oxidation from 0_2 plasma and the probe area is 4.72 mm. It can acquire, analyzes, and present data as graphs or tables with the use its software program ESPsoft made by Hiden. Analysis of the I-V curve in this program is based on the "Orbital Motion Limited" theory which effectively increases the diameter of the tip wire for ions [2].

3.4 Theory

$$I_{es} = -\frac{en\bar{c}_e}{4} = en_e\sqrt{\frac{kT_e}{2\pi m_e}}$$

where: I_{es} is electron current at saturation

e (charge of an electron) = 1.602 E-19 C

n is the number of particles

$\bar{c}_e$ is the average electron velocity

n_e is the number or electrons

k (Boltzman's constant) = 1.38 E-23 J/K

T_e is the electron temperature

m_e (mass of an electron) = 9.11 E-31 kg

The region to the right of the plasma potential with the slightly positive slope is known as the electron saturation region.

When the probe has a slightly negative potential compared to the plasma, some of the electrons are repelled. This causes the exponential curve below the plasma potential.

$$I_e = I_{es} \exp\left(\frac{e(V_p - V_B)}{kT_e}\right)$$

where: I_e is the electron current

V_p is the plasma potential in volts

V_B is the probe potential in volts

T_e is the electron temperature in Kelvin

From this, ln ($I_p + I_i$) can be plotted against V_p to produce a straight line whose slope represents the electron temperature.

The point on the curve that crosses the x-axis (V) is the floating potential ($V_B = V_f$). Here only a small portion of the electrons can overcome the bias potential of the probe. The net current is equal to zero because the electron current is compensated by the ion current.

Finally, when the probe possess a negative potential high enough that no electrons can reach the probe, the ion current (I_{is}) can be measured. Here, only the ion flux is measured by the probe. I_{is} is constant when the bias potential is less than or equal to zero with respect to the plasma [13].

$$I_{is} = eA_p n \exp\left(-\frac{1}{2} * \sqrt{\frac{kT_e}{M_e}}\right)$$

where: A_p is the area of the probe tip = 4.72mm

With this information, the plasma current (I_p) can now be found. This is the current corresponding to the plasma potential (V_p) on the I-V curve.

$$I_p = I_e - I_i = I_{es} \exp\left(\frac{e(V_p - V_B)}{kT_e}\right)$$

The ion flux is another characteristic of plasmas that can be determined with a Langmuir probe. Flux is defined as the number per area per time.

$$\Gamma_i = \frac{n\bar{c}_i}{4}$$

where: Γ_i is ion flux

$\bar{c}_i$ (avg. ion velocity) = $\sqrt{\frac{8KT}{\pi m_i}}$

The characteristic distance in which a charged particle in the plasma is shielded from external electric fields can also be found. This is known as the Debye length.

$$\lambda_D = \sqrt{\frac{\varepsilon_0 KT}{n_e e^2}}$$

where: ε_0 (permittivity of free space) = 8.854 E -12 F/m

n_i is the ion density

[8]

The EEDF can also be calculated. This is done by substituting the second differential values of the I-V curve into the Druyvesteyn equation (ESPsoft User Manual, 8-5)

$$F(\varepsilon) = \frac{4}{e^2 A}\left(\frac{-mV}{2e}\right)^{\frac{1}{2}} \frac{d^2 I}{dV^2}$$

where: $F(\varepsilon)$ is the electron energy distribution function (EEDF)

V = potential (V)

A = current (A)

$\frac{d^2 I}{dV^2}$ are the second differential values

3.5 The Top Plate Design

The top plate of the inverted cylindrical magnetron sputtering system (ICM-10) used in our experiments was not equipped for the state-of-the-art diagnostic instruments (ESP*ION* Langmuir probe and EQP mass spectrometer) used to analyze the plasma in the ICM-10. Some design work was required to enable these systems to be utilized. Both the ESP*ION* and EQP require a probe to be inserted into the plasma for measurement. To make this possible, a new solid top plate had to be designed for the system.

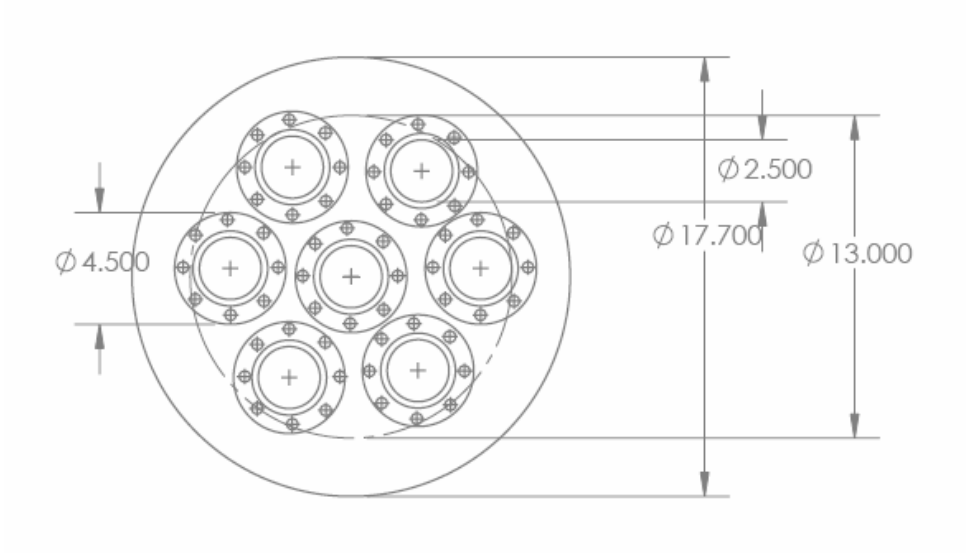

Figure 10: Top plate design 1

The first top plate built and designed includes seven openings in which both the ESP*ION* and EQP (via an adapter) can be inserted and attached. There is one hole in the center and six around the edge progressively one-fifth of an inch further from the outside wall (where the sputtering occurs).

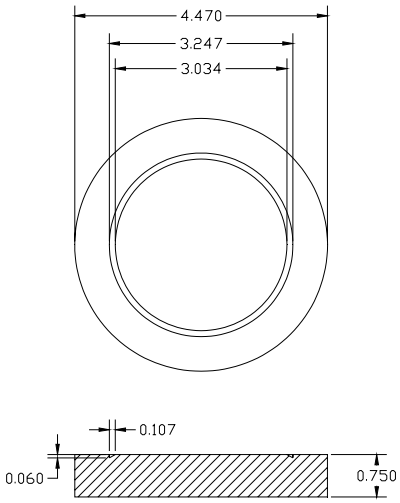

Figure 11: Blank design

Blanks were also designed to occupy the holes not being used to keep the essential vacuum in the ICM.

Unfortunately, the outer holes were to close to the walls/shutter to be safely used with either of the expensive and fragile diagnostic systems. We are currently working on a new top plate with three holes 2", 3", and 4" from the center of the target to the center of the opening. This gives us a clearance of 2" from the shutter on the outermost hole.

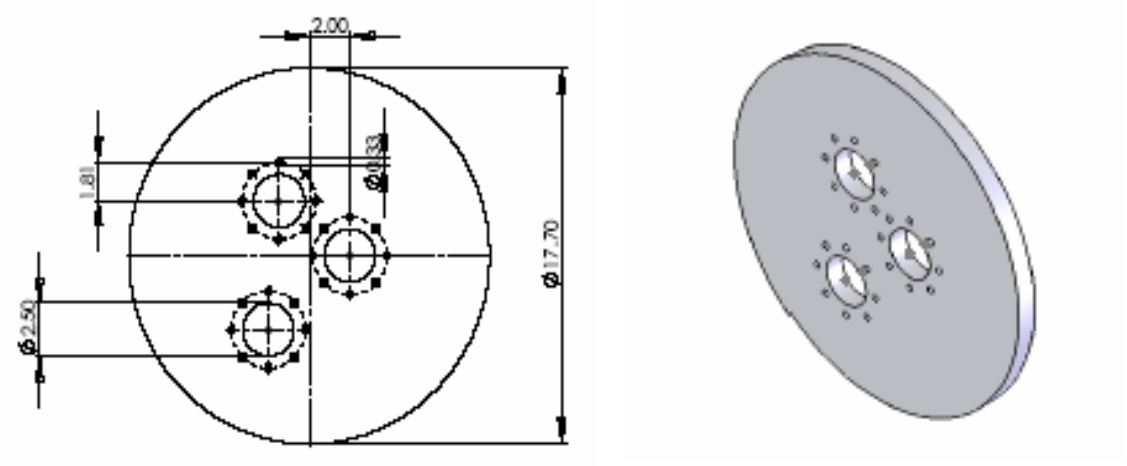

Figure 12: Top plate design 2

Air cooling has also been added to the ESP*ION* system. The first probe used in our system malfunctioned because the temperature inside exceeded the probes limit. The inductors inside the probe melted at about 300˚C. Air pressure at 3-10 psi now runs down the probe during operation to help control the temperature.

Chapter Four

4.0 Results and Discussion

The parameters of the ICM-10 magnetron sputtering system determine the plasmas created within it and ultimately the thin films deposited on the substrate. The specific parameters of the sputtering system are known as a recipe to create each plasma. Two recipes were used throughout this research for plasma characterization by both the EQP and ESP*ION* diagnostic systems. The first was a recipe for low power oxygen plasma

and the second was for low power argon plasma. Low power plasmas had to be used to keep the temperatures sufficient low to prohibit damaging the diagnostic systems. Below are the recipes used to create these plasmas.

Table 2: Low power oxygen plasma recipe

	Step 1	Step 2
Argon (0 - 200 sccm)	80	0
Oxygen (0 - 200 sccm)	45	45
MDX Mode (I/V/P)	V	V
MDX (I = 0-10, V = 0-1000, P = 0-5000)	35	0
PE II Mode (I/V/P)	P	P
PE II (I = 0-35, V = 0-1100, P = 0-10000)	500	500
Shutter (Open/Closed)	Closed	Closed
Step Time (Seconds)	60	3600

Table 3: Low power argon plasma recipe

	Step 1	Step 2
Argon (0 - 200 sccm)	120	60
Oxygen (0 - 200 sccm)	0	0
MDX Mode (I/V/P)	P	P
MDX (I = 0-10, V = 0-1000, P = 0-5000)	0	0
PE II Mode (I/V/P)	P	P
PE II (I = 0-35, V = 0-1100, P = 0-10000)	500	500
Shutter (Open/Closed)	Closed	Closed
Step Time (Seconds)	60	3600

Step 1 for both the oxygen and argon plasma is an ignition step. In the oxygen plasma, both oxygen and argon gas are present because it is difficult to initiate oxygen plasma on its own. Throughout both processes, the power is low (0.5 kW) to prevent high temperatures and the shutter is closed to prevent sputtering. In this preliminary research, our concern is with the plasma characteristics, not the sputtered particles. In the second step, only the gas for the plasma desired (oxygen or argon) is present. The chamber and convectron pressures were roughly 7.3 E -3 torr, while the foreline pressure remained at

about 9.3 E -2 torr throughout both processes. All data for the oxygen and argon plasmas were taken during the second step.

4.1 EQP Data

Figure 13: Experimental system, EQP on ICM-10

One of the useful benefits of the EQP is that it can show exactly what particles are present within your system and if there are any leaks in the vacuum or gas lines. Even when our ICM is pumped down to 10 E -7 torr, some particles are still present. Below is an RGA mass scan with no plasma at vacuum.

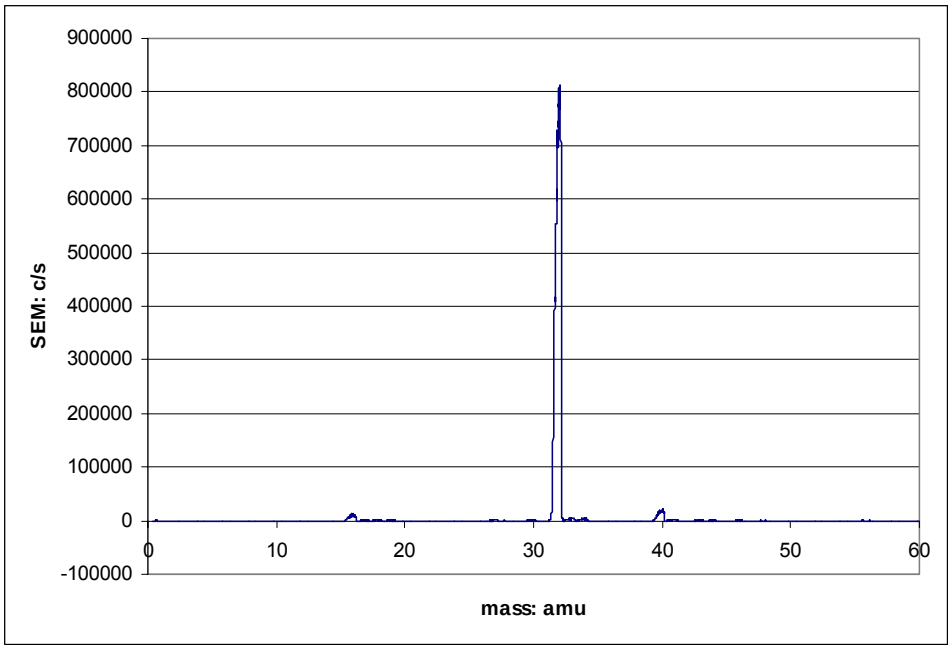

Figure 14: No plasma, RGA mass scan (0-60 amu)

It is obvious that even at vacuum, there are particles present. Oxygen gas (amu = 32) is by far the dominant species here. There is also some O^{16} (amu = 16) and argon gas (amu = 40) in the chamber. The argon gas is probably there because of either a leak in the argon gas line or some is left from previous argon plasma experiments. Either way, there is only a minute quantity present. O_2 is there because it is readily present in our atmosphere.

As stated in the theory, there are two modes of scanning that can be taken with the EQP. The RGA scan is for sampling neutrals and radicals and the SIMS scan is for positive and negative ions. Within each of those modes, an energy and mass scan can be taken simultaneously. The first set of scans to be examined is with low-power oxygen plasma. Because oxygen gas is being used to create the plasma, 0_2 is the most common element in the system. It was necessary on the mass scans to break the scan into segments in order

to miss the 30-35 amu range because 0_2 has a mass of 32 amu. If this range were measured (as shown below), the rest of the data range is dwarfed by the high oxygen count and the results are not detailed enough to be useful.

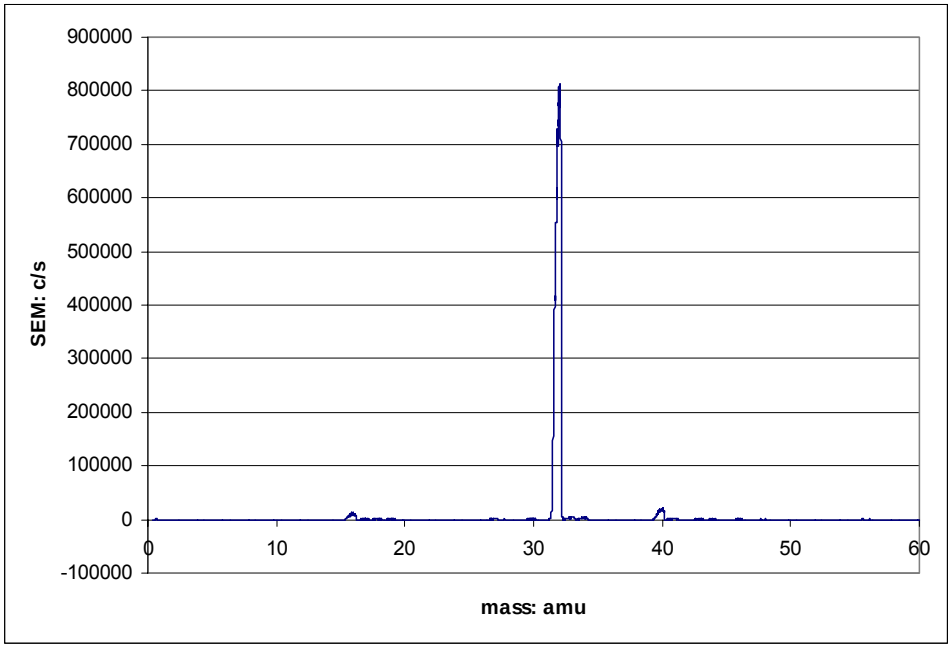

Figure 15: Oxygen plasma, SIMS positive ion mass scan (0-60 amu)

The RGA mass scan was broken into three segments (0-16, 16-30, & 30-60 amu) for greater detail and to purposely miss the 32 amu section.

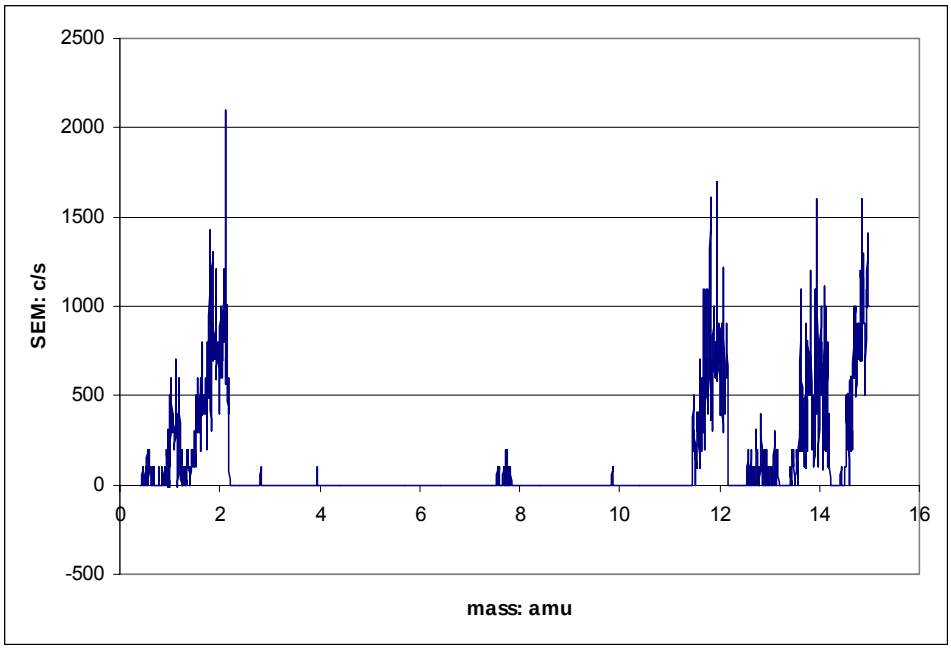

Figure 16: Oxygen plasma, RGA mass scan (0-16 amu)

In the 0-16 amu range, it appears that some hydrogen gas (H_2, amu = 2), carbon (C^{12}, amu = 12), and nitrogen gas (N_2, amu = 14) are present. Even if so, their presence is negligible because their counts per second (c/s) is so small (2 E+3) compared to some of the major elements and compounds present (7 E+6 c/s).

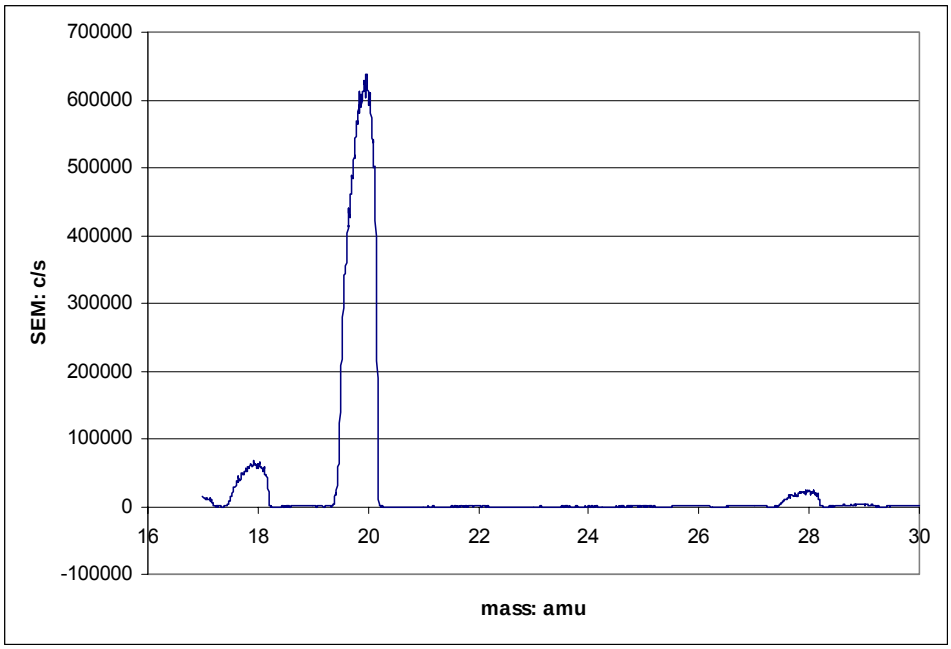

Figure 17: Oxygen plasma, RGA mass scan (16-30 amu)

In the 16-30 amu range, some water (H_20, amu = 18) and nitrogen gas (N_2, amu = 28) are present. However, there is far more Ar^{20} (amu = 20) than anything else in that range.

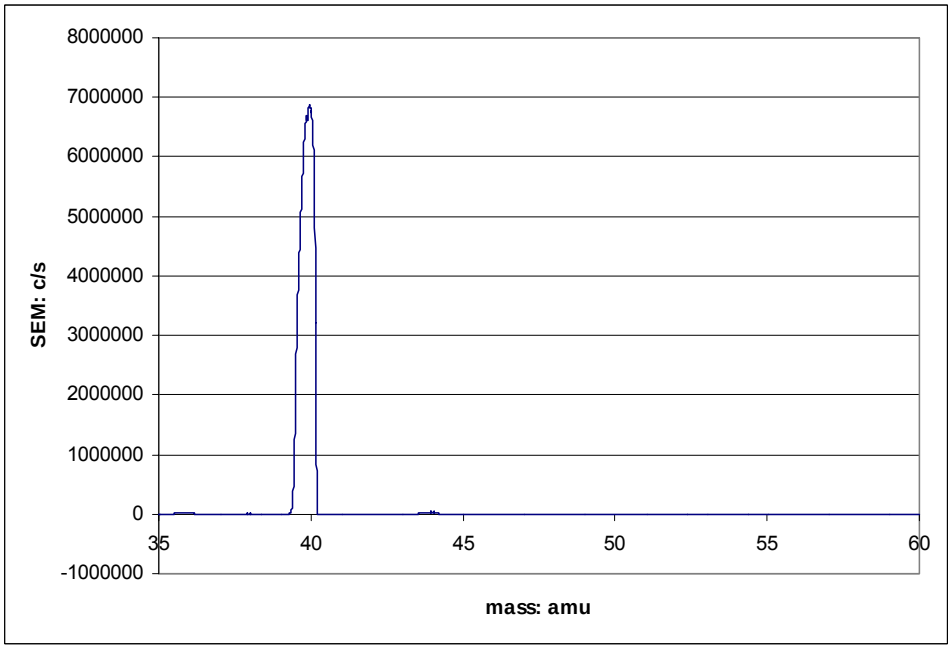

Figure 18: Oxygen plasma, RGA mass scan (35-60 amu)

The last range from 35-60 amu contains Argon (amu = 40) which has a c/s of a whole order of magnitude greater than any other. There also appears to be some carbon dioxide ($C0_2$, amu = 44), but it is hard to see because it has such a smaller count compared to Ar. For comparison, here is a RGA scan of argon plasma created with the recipe described earlier.

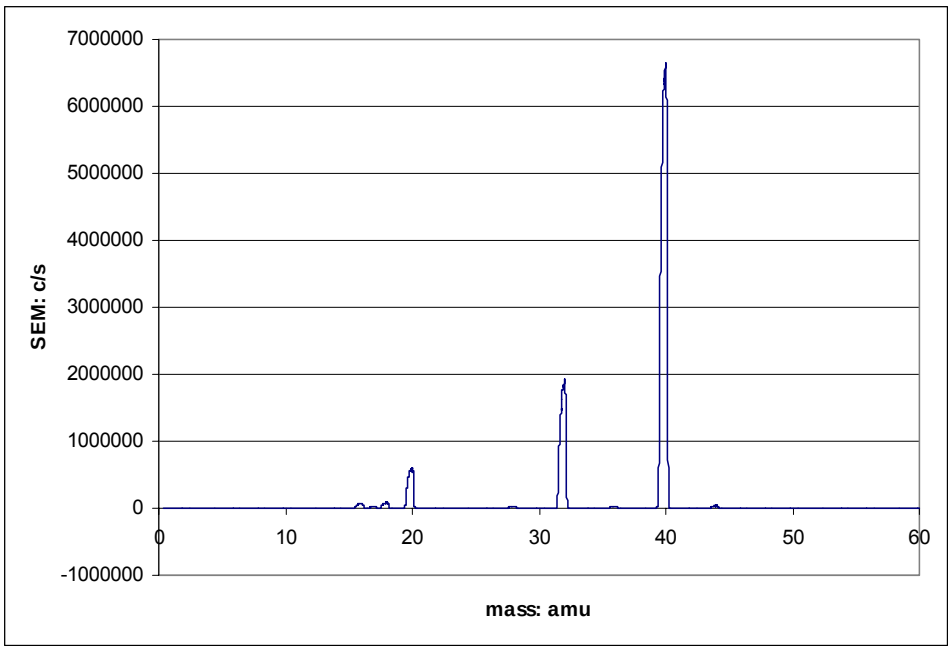

Figure 19: Argon plasma, RGA mass scan (0-60 amu)

Argon gas is the dominant species as expected followed by oxygen gas and Ar^{20}. Argon had a similar count in both the oxygen plasma and argon plasma RGA scans at just under 7 E+6 c/s. Obviously there is much less oxygen gas in the argon plasma as in the oxygen plasma (which was not shown). Both scans also showed particles present at a mass of 20, 18, and 16 amu.

The RGA oxygen plasma energy scan below shows the energy in Volts against the c/s so that one can determine the energy of an element or compound by matching its c/s in the mass scan.

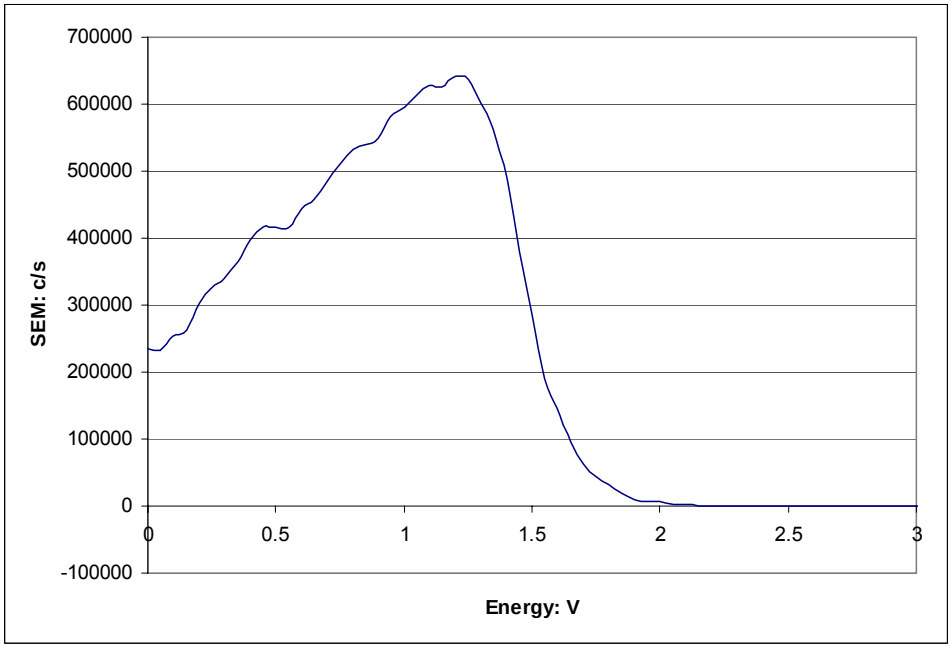

Figure 20: Oxygen plasma, RGA energy scan

For example, the peak of this RGA is at about 6.3 E+5 c/s which corresponds to Ar^{20}. We can now see that the charge on that compound is about 1.25 volts.

A SIMS positive ion scan was also done on this same oxygen plasma. The mass scan was broken into two parts, 0-30 and 35-60 amu, again to miss oxygen gas ions at 32 amu.

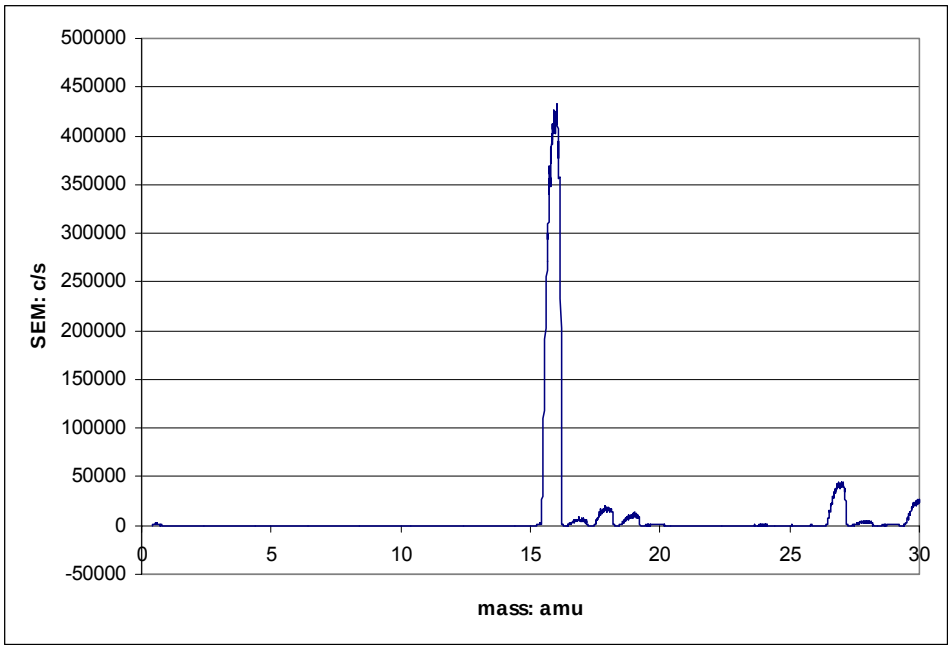

Figure 21: Oxygen plasma, SIMS positive ion mass scan (0-30 amu)

Obviously, oxygen (O^{16}, amu = 16) is the most abundant species in this range. This is followed by what appears to be aluminum (Al^{27}, amu = 27), which could have possibly sputtered of the aluminum target and made its way around the shutter. Still it has a very low c/s and therefore is relatively unimportant.

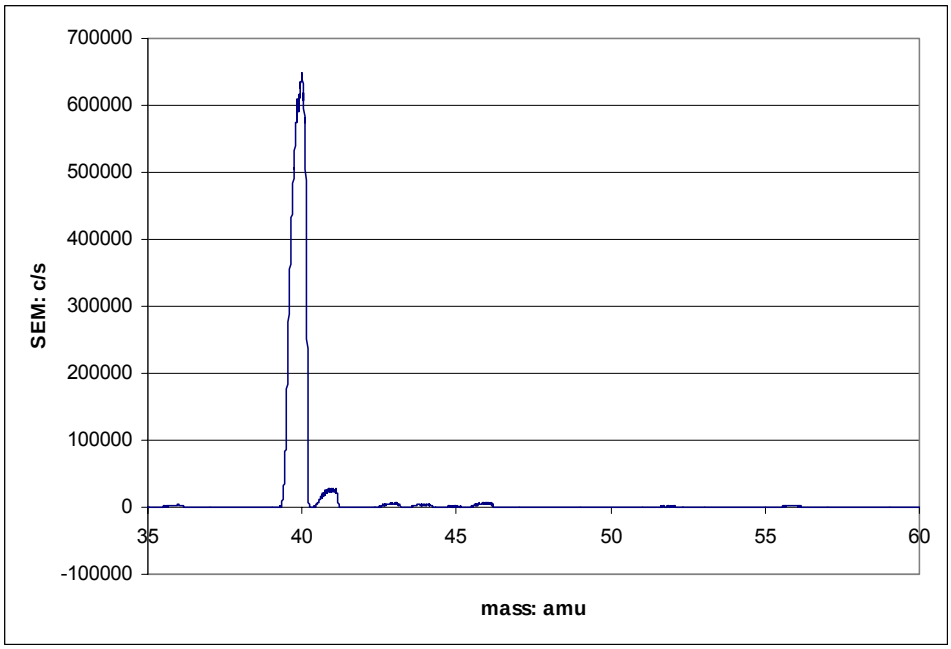

Figure 22: Oxygen plasma, SIMS positive ion mass scan (35-60 amu)

Again, as in the RGA mass scan, Argon is the most abundant species, other than oxygen of course. Because this is a positive ion scan, this shows that argon had the most negatively ionized atoms in this plasma.

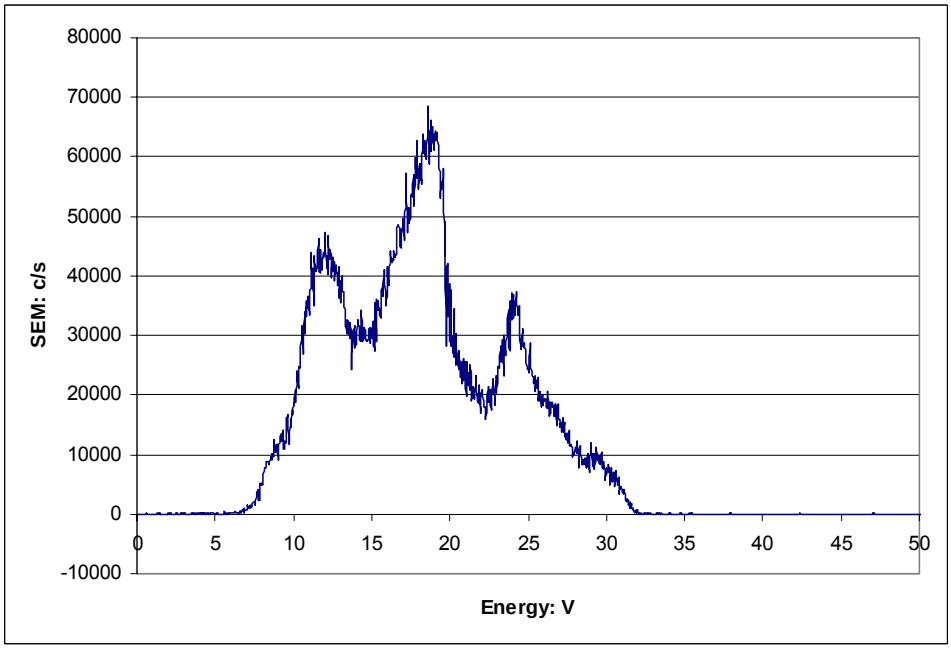

Figure 23: Oxygen plasma, SIMS positive ion energy scan

It is easily recognized that the SIMS ion energy scan has a much higher energy than the RGA scan which makes sense because ions possess a charge while the neutrals don't. Also, from this graph one can see that the energy is coming from elements and compounds with low c/s in the 0-70,000 range. This data helps to determine what species and the amount present for a specific plasma.

4.2 ESP*ION* Data

As discussed in the theory, a Langmuir probe measures current produced in a plasma as a function of the probes bias voltage. This produces a current-voltage (I-V) curve which is used to find the plasmas' potential (V_p), floating potential floating potential, electron temperature (T_e), electron density (N_e), ion density (N_i), Debye length (λ_D), ion flux, and electron energy distribution function (EEDF). Our ESPION Langmuir probe uses the ESPsoft program both made by Hiden to collect and process the data taken. This ESPION also has a translating z-drive that is capable of taking measurements over a range of 30cm, which covers the entire height of our sputtering system.

In this first set of data, oxygen plasma was sampled at three different locations within our system. The three locations represent the centers of the three targets (aluminum).

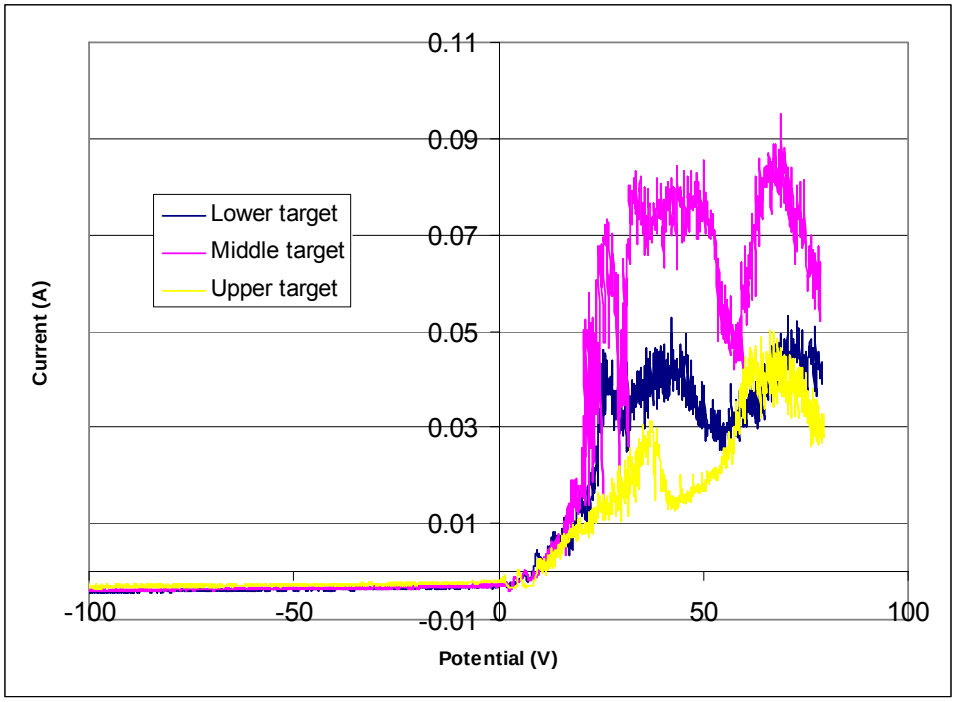

Figure 24: Oxygen plasma at 3 targets (I-V curve)

The center of the lower target is about 25 cm from the top, the middle target (not active) is roughly 16.5 cm from the top, and the upper target is about 5.1 cm from the top. The graph produced represents the three I-V curves of the oxygen plasma at each location. While this data is odd because of the jagged spikes on the upper right portion of the graph, it is very interesting because of the obvious differences at each target center. It is believed that the plasma should be uniform through the cylindrical sputtering system.

The graph below shows what kind of results one would expect to see from an I-V curve and its first and second differential.

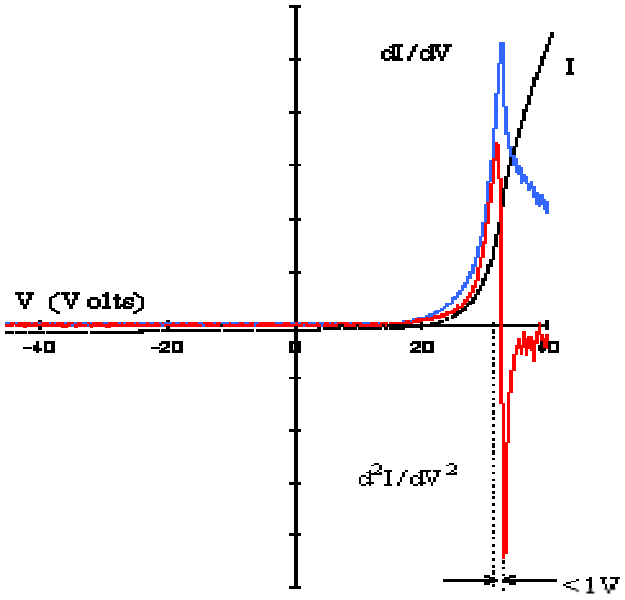

Figure 25: Example of typical I-V, first, and second differential curves [3]

The regular I-V curve has an "I" to its right and is a smooth curve that has a slightly positive slope just below the x-axis (voltage) and turns up into an s-shaped exponential curve as it crosses and normally flats back out again after the floating potential. The second differential has the "dI/dV" to its left and follows closely to the I-V curve until it spikes and sharply turns down. Lastly, the second differential curve with the "d^2I/dV^2" to its left again follows closely to the I-V curve's path but spikes lower than the first differential and has a minimum spike below the x-axis. The second differential is used to produce a EED function which is represented in example below.

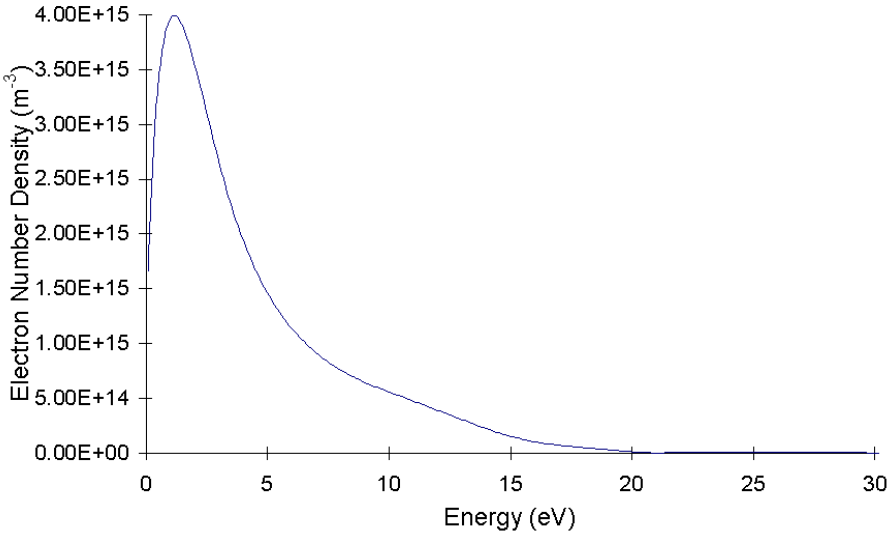

Figure 26: Example of typical EED function [3]

To produce more accurate and consistent data, we took multiple scans at one time, averaged them, and produced a smoothed curve with the ESPION and ESPsoft system.

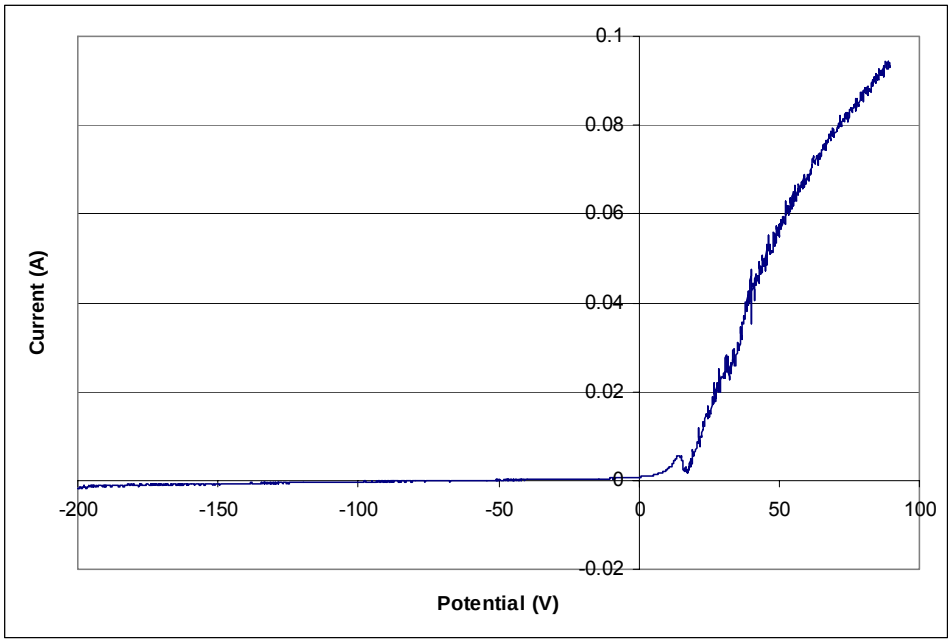

Figure 27: Oxygen plasma, 8 scan avg. (I-V curve)

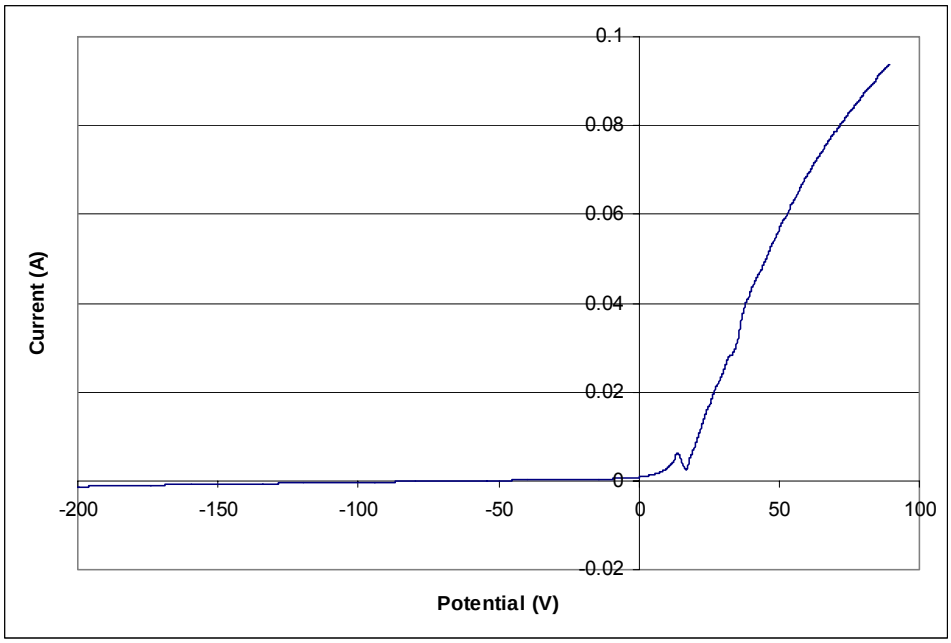

Figure 28: Oxygen plasma, smooth curve (I-V curve)

The first graph is an average of 8 scans of oxygen plasma taken at one time and the second is of the same data with a smooth curve. The graph produced is fairly consistent with what one would expect to see on an I-V curve with the exception of the small minimum and maximum spikes near the origin. The cause of this has not yet been discovered and will be continued to be researched. The I-V curve produced from the oxygen plasma recipe gave us these experimental plasma conditions:

Table 4: Oxygen plasma results

Floating Potential	-14.88	V
Plasma Potential (Vp)	23.33	V
Electron Temperature (Te)	4.42E+04	K
Electron Temperature (Te)	3.81	eV
Electron Density (Ne)	1.41E+17	m^-3
Ion Density (Ni)	2.05E+17	m^-3
Debye Length (λD)	3.87E-05	m
Ion Flux	6.18E+20	m^2*s

From the smooth I-V curve, a graph of the first differential was produced.

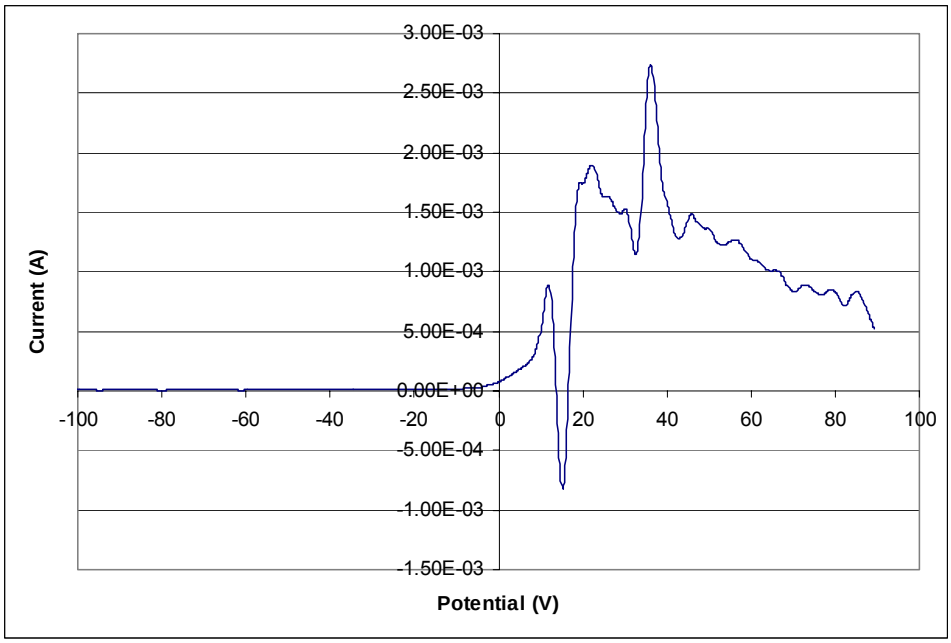

Figure 29: Oxygen plasma, 1st differential

This graph follows a very unusual path. While the beginning and end of the graph display what one would expect to see, the middle is full of unexpected peaks and valleys that are most likely a result of improper data acquisition or damages sustained to our probe at high power.

A differential was taken again from this graph to produce the second differential curve which again displayed unexpected results.

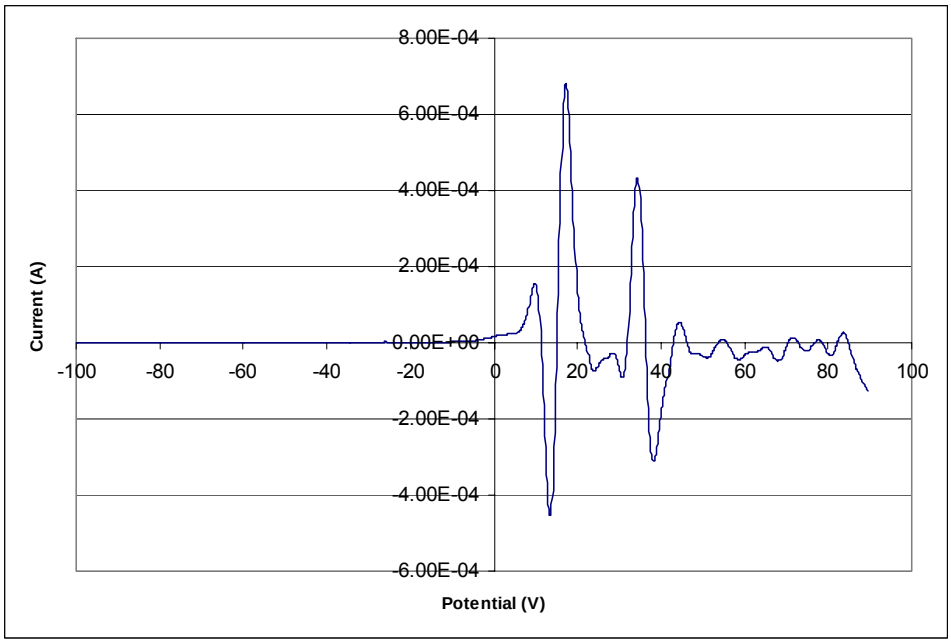

Figure 30: Oxygen plasma, 2nd differential

There should be only one major maximum and minimum, not two or three. Hopefully, as research continues, better data will be collected to produce more clear results. Nevertheless, an EEDF function and its results were produced from this data.

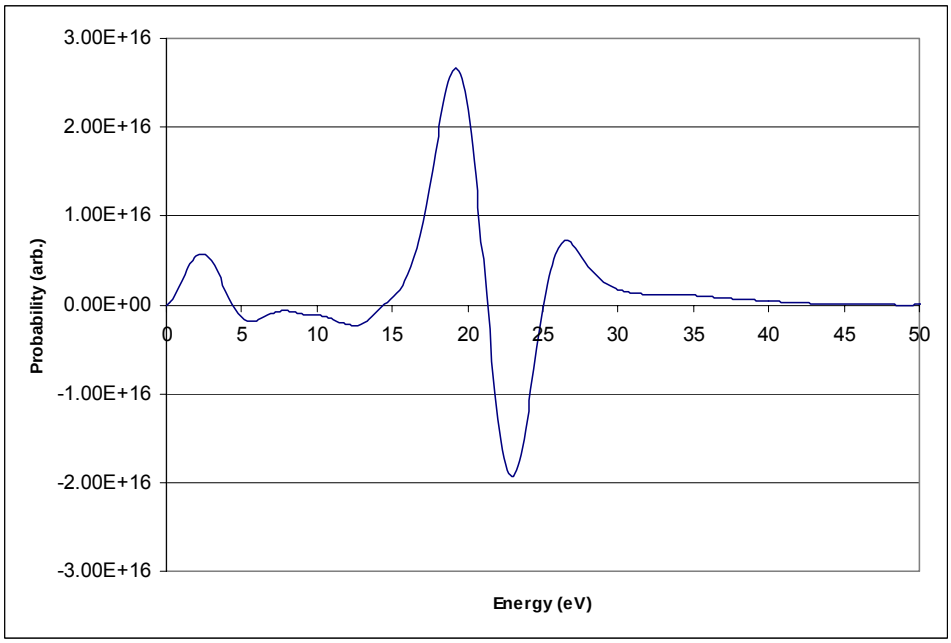

Figure 31: Oxygen plasma EED function

Table 5: Oxygen plasma EEDF results

Floating Potential	-14.88	V
EED (Ne)	7.43E+16	m^-2
EED (Avg. Energy)	19.7	eV
EED (Te)	13.2	eV

The same scans were done on argon plasma for comparison. Below are I-V and EED graphs of argon plasma with their respective results.

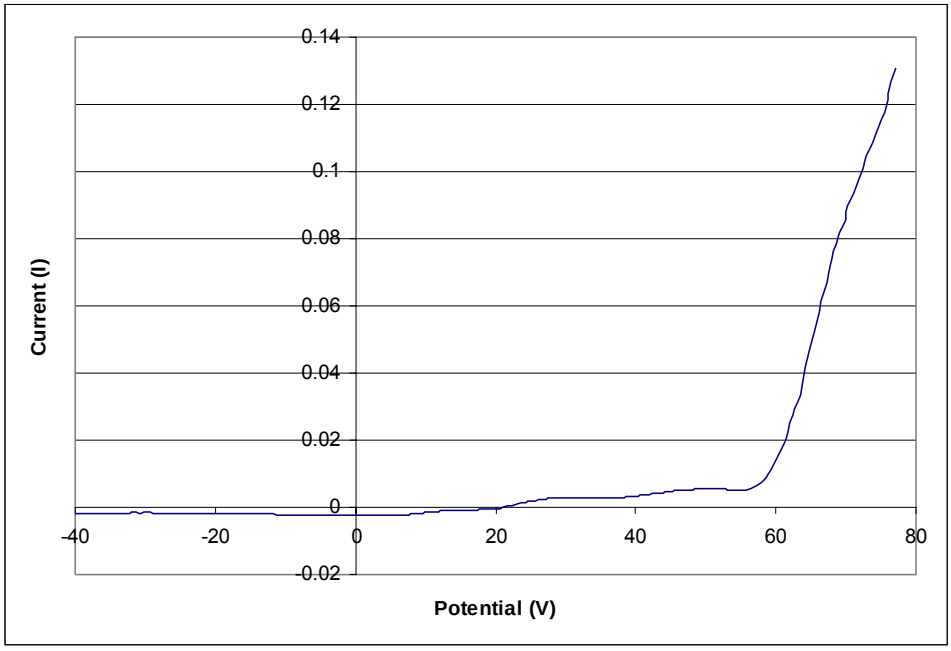

Figure 32: Argon plasma, smooth curve (I-V Curve)

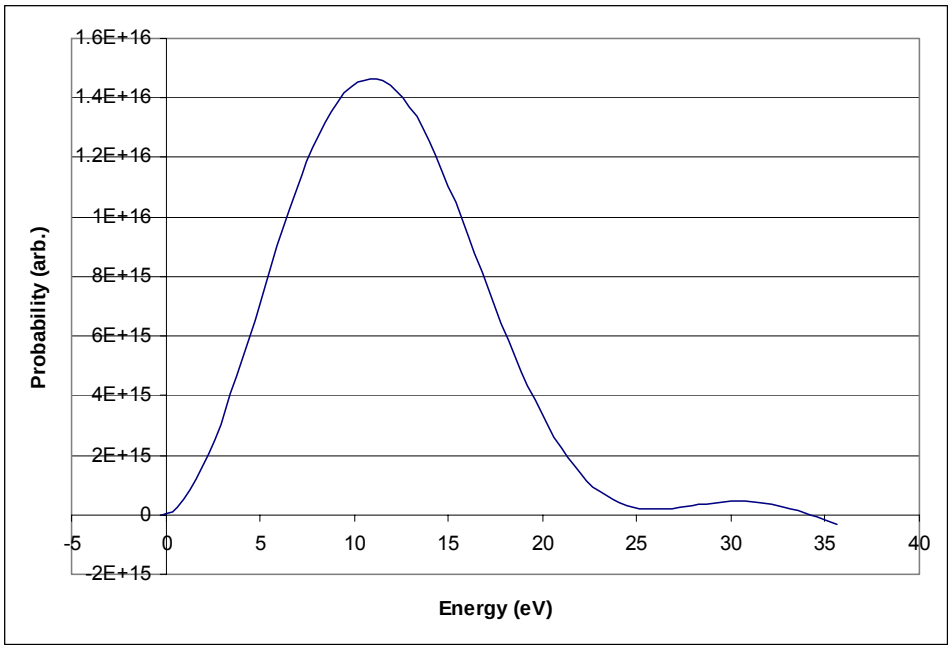

Figure 33: Argon plasma, EED function

Table 6: Argon plasma results

Floating Potential	26.07	V
Plasma Potential	65.4	V
Electron Temperature (Te)	3.97E+04	K
Electron Temperature (Te)	3.43	eV
Electron Density (Ne)	2.74E+17	m^-3
Ion Density (Ni)	0	m^-3
Debye Length (λD)	2.63E-05	m
Ion Flux	0	m^2*s

Table 7: Argon plasma EED function results

Floating Potential	26.07	V
EED (Ne)	1.89E+17	m^-2
EED (Avg. Energy)	11.5	eV
EED (Te)	7.69	eV

The I-V curve produced by the argon plasma was much better and did not contain any unexpected spikes. This also resulted in the EED function being much smoother and more of what one would expect to produce.

Comparing the oxygen and argon plasma results shows us some similarities and differences between them. The plasma potential of the argon is more than double that of the oxygen plasma at 65.4 V compared to 23.33 V. Their electron temperatures were fairly similar with oxygen plasma having a high temperature of only 0.38 eV. The electron density of the argon plasma was again almost double that of the oxygen, but the argon plasma showed no ion density or ion flux which doesn't seem possible. The Debye length of the argon was also a third less than the oxygen's.

Chapter Five

5.0 Conclusions

The primary goals of my research were to create preliminary characterization of the plasma conditions in our inverted cylindrical magnetron sputtering system by learning how our plasma diagnostic systems work, how to operate them, and how to produce data. All of the data and results were experimental and have neither been proved nor disproved. Others that follow will continue with this research and follow this ground work. They will learn to prefect the data acquisition process, create useable data, interpret the data correctly, and produce a true characterization of our system.

Many possible factors could have contributed to results being skewed or false. One of the major possibilities is that both systems (ESP*ION* and EQP) were not equipped to operate at the high temperatures produced in our system. All of the data for this report was produced was at low power (.5 KW) and temperatures (<300˚C) because both systems malfunctioned before high power (5 KW) could be achieved. Higher

temperature probes are being obtained and both systems will be incorporated with water cooling which should allow for higher power operation. Novelty and our unfamiliarity of these complex systems could have also played a role in imperfect data. This could have contributed to the noise that was seen within the data. This problem should decrease as more time is spent operating these plasma diagnostic systems.

Interpretation of the data is a final vital step in this research. Interpretation is very difficult and can be futile with preliminary data that is unproven. This will become more important as these diagnostic techniques are perfected through time and practice. As more data is collected consistently, interpretation will become more realistic as one can compare and contrast results with similar and different parameters. Finally, no one really knows what results should be seen within this system. That is the whole premise of this research. Rough assumptions can be made, but we will not know for sure until the diagnostic techniques are perfected and the data is interpreted properly. Once this is done, correlations can be made between the deposition parameters, the plasma characteristics present, and the quality of the material deposited. With this information, it will be possible to fully understand exactly what materials are being deposited and more importantly why. My research should help us to move towards this goal.

5.1 Future Work

Research will continue with all three systems (ICM-10, ESP*ION* and EQP) discussed in this paper. The first thing to be done will be adding water-cooling to both the ESP*ION* and EQP. Both systems are exceeding their maximum operating temperatures and can

not take measurements at high power. This is desired because the plasma needed to grow α-alumina is created at high power (5 kW). Up to this point, measurements have only been taken at lower power and temperatures. The ESP*ION* probe was recently sent back to Hiden Analytical and the EQP is soon to follow.

Two new top plates will also be needed to accommodate the water-cooled mass spectrometer. Because the modified probe will possess a larger diameter, the new designs can include only one or two openings. The first new top plate will have only one large opening in center for the EQP. The second will include two openings near the outer wall, one for the EQP and one for the ESP*ION*. The opening will be as close to the wall as possible (about one inch from the shutter).

Plasma diagnostic research will be continued on the ICM-10 with the ESP*ION* and EQP. As more experiments are performed, a better understanding of how to perform the processes and collect good data will be gained. Once these diagnostic processes are perfected, the next step will be to learn to correctly interpret the data. With good data that can be properly interpreted, the final goal of correlating what specific parameters and plasma conditions result in what quality of deposition can be achieved.

Works Cited

[1] Backer, Hermann. Time-Resolved Measurements of Pulsed Plasma for Thin Film Deposition. University of Manchester Institute of Science and Technology. 2003. 1-67.

[2] ESPsoft Users Manual. Hiden Analytical. 2000. 8_5-8_8.

[3] EQP/EQS Analyser Operator's Manual. Warrington: Hiden Analytical Limited. 1_5-5_7.

[4] F, Debal, Bretagne J, and Jumet M. Analysis of DC Magnetron Discharges in Ar-N2 Gas Mixtures. University of Mons-Hainaut, University of Paris-Sud. 1998.

[5] F, Debal, Bretagne J, Wautelet M, Dauchot J P, and Hecq M. Analysis of DC Magnetron Discharges in Ar-N2 Gas Mixtures. Comparison of a Collisional-Radiative Model with Optical Emission Spectroscopy. University of Mons-Hainaut, University of Paris-Sud. 1998. 219-220.

[6] Glocker, David, D. Hofmann, A. Feuerstein, H. Schussler, M. M. Romach, and V. W. Lindberg. ICM10. 2001.

[7] "Hiden ESPION Series Electrostatic Plasma Probes." Hiden Analytical. 5 June-July 2007 <www.hidenanalytical.com>.

[8] Kruger, Charles H., and W. G. Vincenti. Physical Gas Dynamics. Malabar Florida: Krieger Co., 1967. 1-210.

[9] "Mass Spectrometry of Processing Plasmas Using the Hiden EQP System." Hiden Analytical. 5 June-July 2007 <www.hidenanalytical.com>.

[10] "Quadrupole Mass Spectrometry Concepts." Hiden Analytical. 5 June-July 2007 <www.hidenanalytical.com>.

[11] Seo, Sang-Hun, and Jeon-Geon Han. Effect of Duty Cycle on Plasma Parameters in the Pulsed De Magnetron Argon Discharge. Korea Advanced Institute of Science and Technology. 2005.

[12] Srivastava, Abhishek. Optical Emission Spectroscopy in an Inverted Cylindrical Magnetron Plasma. University of Arkansas. 2006. 3-12.

[13] Vetushka, Alena. Study of the Plasma Parameters in a Bi-Polar Pulsed Magnetron Discharge. University of Manchester. 2006. 14-49.

Appendix A: Common atomic weights from Hiden Analytical, Inc.

HIDEN ANALYTICAL

ATOMIC WEIGHTS OF THE ELEMENTS BASED ON THE CARBON 12 STANDARD

Symbol	Amu	Abundance	Symbol	Amu	Abundance
H^{1}	1.0078	99.99	Ca^{40}	39.9626	96.92
H^{2}	2.0141	0.02	Ca^{42}	41.9586	0.64
He^{3}	3.0160	0.00013	Ca^{43}	42.9588	0.13
He^{4}	4.0026	100.00	Ca^{44}	43.9555	2.13
Li^{6}	6.0151	7.52	Ca^{46}	45.9537	0.0032
Li	7.0160	92.48	Ca^{48}	47.9525	0.18
Be^{9}	9.0123	100.00	Sc^{45}	44.9559	100.00
B^{10}	10.0129	18.98	Ti^{46}	45.9526	7.95
B^{11}	11.0093	81.02	Ti^{47}	46.9518	7.75
C^{12}	12.0000	98.89	Ti^{48}	47.9479	73.45
C^{13}	13.0034	1.11	Ti^{49}	48.9479	5.51
N^{14}	14.0031	99.64	Ti^{50}	49.9448	5.34
N^{15}	15.0001	0.37	V^{50}	49.9472	0.24
O^{16}	15.9949	95.77	V^{51}	50.9440	99.76
O^{17}	16.9991	0.04	Cr^{50}	49.9460	4.31
O^{18}	17.9992	0.20	Cr^{52}	51.9405	83.76
F^{19}	18.9984	100.00	Cr^{53}	52.9406	9.55
Ne^{20}	19.9924	90.92	Cr^{54}	53.9389	2.38
Ne^{21}	20.9939	0.26	Mn^{55}	54.9381	100.00
Ne^{22}	21.9914	8.82	Fe^{54}	53.9306	5.90
Na^{23}	22.9898	100.00	Fe^{56}	55.9349	91.52
Mg^{24}	23.9350	78.60	Fe^{57}	56.9354	2.25
Mg^{25}	24.9858	10.11	Fe^{58}	57.9333	0.33
Mg^{26}	25.9826	11.29	Co^{59}	58.9332	100.00
Al^{27}	26.9815	100.00	Ni^{58}	57.9354	67.76
Si^{28}	27.9769	92.18	Ni^{60}	59.9308	26.16
Si^{29}	28.9765	4.71	Ni^{61}	60.9311	1.25
Si^{30}	29.9738	3.12	Ni^{62}	61.3283	3.66
P^{31}	30.9738	100.00	Ni^{64}	63.9280	1.16
S^{32}	31.9721	95.02	Cu^{63}	62.9296	69.09
S^{33}	32.9715	0.75	Cu^{65}	64.9278	30.91
S^{34}	33.9679	4.22	Zn^{64}	63.9291	48.89
S^{36}	35.9671	0.11	Zn^{66}	65.9260	27.81
Cl^{35}	34.9689	75.40	Zn^{67}	66.9271	4.11
Cl^{37}	36.9659	24.60	Zn^{68}	67.9249	18.56
A^{36}	35.9675	0.34	Zn^{70}	69.9253	0.62
A^{38}	37.9627	0.063	Ga^{69}	68.9257	60.20
A^{40}	39.9624	99.60	Ga^{71}	70.9248	39.80
K^{39}	38.9637	93.08	Ge^{70}	69.9240	20.52
K^{40}	39.9640	0.012	Ge^{72}	71.9216	27.43
K^{41}	40.9618	6.91	Ge^{73}	72.9233	7.76

Symbol	Amu	Abundance
Ge^{74}	73.9210	36.54
Ge^{76}	75.9213	7.76
As^{75}	74.9217	100.00
Se^{74}	73.9225	0.96
Se^{76}	75.9193	9.12
Se^{77}	76.9200	7.50
Se^{78}	77.9174	23.61
Se^{80}	79.9165	49.96
Se^{82}	81.9166	8.94
Br^{79}	78.9184	50.57
Br^{81}	80.9164	49.43
Kr^{78}	77.9202	0.35
Kr^{80}	79.9166	2.27
Kr^{82}	81.9135	11.56
Kr^{83}	82.9141	11.65
Kr^{84}	83.9115	56.90
Kr^{86}	85.9108	17.37
Rb^{85}	84.9120	72.15
Rb^{87}	86.9093	27.85
Sr^{84}	83.9133	0.56
Sr^{86}	85.9094	9.86
Sr^{87}	86.9090	7.02
Sr^{88}	87.9060	82.56
Y^{89}	88.9057	100.00
Zr^{90}	89.9043	51.46
Zr^{91}	90.9053	11.23
Zr^{92}	91.9047	17.11
Zr^{94}	(98.9076)	17.40
Zr^{96}	95.9093	2.80
Nb^{93}	92.9057	100.00
Mo^{92}	91.9086	15.05
Mo^{94}	93.9059	9.35
Mo^{95}	94.0944	14.78
Mo^{96}	95.9050	16.56
Mo^{97}	96.9062	9.60
Mo^{98}	97.9060	24.00
Mo^{100}	99.9065	9.68
Ru^{96}	95.9087	5.68
Ru^{98}	(97.9540)	2.22
Ru^{99}	98.9061	12.81
Ru^{100}	(99.9050)	12.70
Ru^{101}	(100.9050)	16.98
Ru^{102}	101.9037	31.34
Ru^{104}	103.9042	18.27
Rh^{103}	102.9046	100.00
Pd^{102}	101.9049	0.80
Pd^{104}	103.9033	9.30
Pd^{105}	104.9042	22.60
Pd^{106}	105.9029	27.10
Pd^{108}	107.9035	26.70
Pd^{110}	109.9045	13.50
Ag^{107}	106.9048	51.35
Ag^{109}	108.9046	48.65
Cd^{106}	105.9059	1.22
Cd^{108}	107.9041	0.89
Cd^{110}	109.9033	12.43
Cd^{111}	110.9043	12.86
Cd^{112}	111.9031	23.79
Cd^{113}	112.9045	12.34
Cd^{114}	113.9036	28.81
Cd^{116}	115.9050	7.66
In^{113}	112.9043	4.16
In^{115}	114.9036	95.84
Sn^{112}	111.9051	0.95
Sn^{114}	113.9039	0.65
Sn^{115}	114.9034	0.34
Sn^{116}	115.9022	14.24
Sn^{117}	116.9031	7.67
Sn^{118}	117.9021	24.01
Sn^{119}	118.9032	8.58
Sn^{120}	119.9022	32.97
Sn^{122}	121.9035	4.71
Sn^{124}	123.9052	5.98
Sb^{121}	120.9037	57.25
Sb^{123}	122.9042	42.75
Te^{120}	119.9045	0.09
Te^{122}	121.9029	2.46
Te^{123}	122.9043	0.87
Te^{124}	123.9001	4.61
Te^{125}	124.9046	6.83
Te^{126}	125.9039	18.71
Te^{128}	127.9056	31.79
Te^{130}	129.9070	34.49
I^{127}	126.9047	100.00
Xe^{124}	123.9061	0.10
Xe^{126}	125.9045	0.09
Xe^{128}	127.9035	1.92
Xe^{129}	128.9047	26.44
Xe^{130}	129.9035	4.08
Xe^{131}	130.9051	21.18
Xe^{132}	131.9042	26.89

Symbol	Amu	Abundance	Symbol	Amu	Abundance
Xe^{134}	133.9054	10.44	Dy^{161}	160.9257	18.88
Xe^{136}	135.9072	8.87	Dy^{162}	161.9256	25.53
Cs^{133}	132.9051	100.00	Dy^{163}	162.9278	24.87
Ba^{130}	129.9062	0.10	Dy^{164}	163.9285	28.18
Ba^{132}	131.9051	0.10	Ho^{165}	164.9291	100.00
Ba^{134}	133.9043	2.42	Er^{162}	161.9287	0.14
Ba^{135}	134.9056	6.59	Er^{164}	163.9298	1.56
Ba^{136}	135.9044	7.81	Er^{166}	165.9287	33.41
Ba^{137}	136.0956	11.32	Er^{167}	166.9305	22.94
Ba^{138}	137.9049	71.66	Er^{168}	167.9308	27.07
La^{138}	137.9067	0.09	Er^{170}	169.9356	14.88
La^{139}	138.9060	99.91	Tm^{169}	168.9343	100.00
Ce^{136}	135.9071	0.19	Yb^{168}	167.9339	0.14
Ce^{138}	137.9060	0.25	Yb^{170}	(169.9340)	3.03
Ce^{140}	139.9053	88.48	Yb^{171}	(170.9360)	14.31
Ce^{142}	141.9093	11.07	Yb^{172}	(171.9252)	21.82
Pr^{141}	140.9075	100.00	Yb^{173}	(172.9380)	16.13
Nd^{142}	141.9075	27.09	Yb^{174}	(173.9256)	31.84
Nd^{143}	142.9096	12.14	Yb^{176}	(175.9427)	12.73
Nd^{144}	143.9098	23.83	Lu^{175}	(174.9420)	97.40
Nd^{145}	144.9121	8.29	Lu^{176}	175.9419	2.60
Nd^{146}	145.9127	17.26	Hf^{174}	(173.9390)	0.20
Nd^{148}	147.9165	5.74	Hf^{176}	175.9408	5.23
Nd^{150}	149.9208	5.63	Hf^{177}	176.9425	18.55
Sm^{144}	143.9117	3.16	Hf^{178}	177.9430	27.23
Sm^{147}	146.9145	15.07	Hf^{179}	178.9452	13.79
Sm^{148}	147.9144	11.27	Hf^{180}	179.9461	35.07
Sm^{149}	148.9168	13.84	Ta^{180}	179.9450	0.01
Sm^{150}	149.9169	7.47	Ta^{181}	180.9458	99.99
Sm^{152}	151.9194	26.63	W^{180}	179.9445	0.13
Sm^{154}	153.9219	22.53	W^{182}	181.9460	26.31
Eu^{151}	150.9195	47.77	W^{183}	182.9481	14.28
Eu^{153}	152.9206	52.23	W^{184}	183.9489	30.64
Gd^{152}	151.9194	0.20	W^{186}	185.9507	28.64
Gd^{154}	153.9209	2.15	Re^{185}	(184.9480)	37.07
Gd^{155}	154.9227	14.73	Re^{187}	(186.9530)	62.93
Gd^{156}	155.9223	20.47	Os^{184}	(183.9460)	0.02
Gd^{157}	156.9241	15.68	Os^{186}	(185.9520)	1.59
Gd^{158}	157.9244	24.87	Os^{187}	(186.9560)	1.64
Gd^{160}	159.9272	21.90	Os^{188}	(187.9569)	13.20
Tb^{159}	158.9249	100.00	Os^{189}	(188.9585)	16.10
Dy^{156}	(155.9140)	0.05	Os^{190}	(189.9548)	26.40
Dy^{158}	157.9240	0.09	Os^{192}	(191.9622)	41.00
Dy^{160}	159.9239	2.29	Ir^{191}	(190.9634)	38.50

Symbol	Amu	Abundance
Ir^{193}	(192.9667)	61.50
Pt^{190}	(189.9640)	0.012
Pt^{192}	(191.9648)	0.78
Pt^{194}	(193.9633)	32.80
Pt^{195}	(194.9662)	33.70
Pt^{196}	(195.9671)	25.40
Pt^{198}	197.9646	7.23
Au^{197}	196.9672	100.00
Hg^{196}	195.9658	0.15
Hg^{198}	197.9667	10.02
Hg^{199}	198.9682	16.84
Hg^{200}	199.9683	23.13
Hg^{201}	200.9703	13.22
Hg^{202}	201.9706	29.80
Hg^{204}	203.9735	6.85
Tl^{203}	202.9719	29.50
Tl^{205}	204.9738	70.50
Pb^{204}	203.9731	1.37
Pb^{206}	205.9744	25.15
Pb^{207}	206.9759	21.11
Pb^{208}	207.9766	52.38
Bi^{209}	208.9743	100.00
Th^{232}	232.0380	100.00
U^{234}	234.0403	0.01
U^{235}	235.0428	0.72
U^{238}	238.0486	99.28

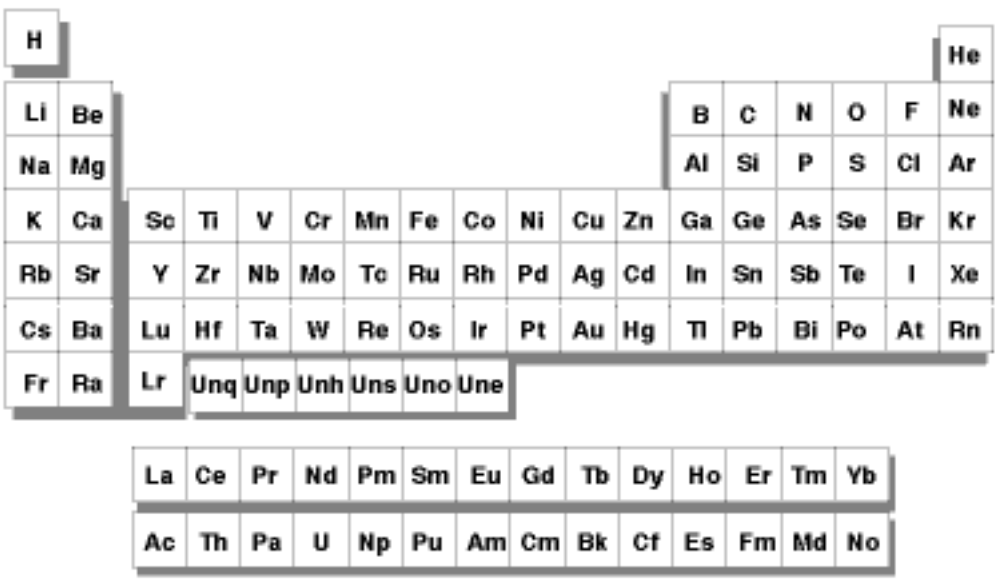

HIDEN ANALYTICAL

Hiden Analytical
420 Europa Boulevard
Warrington
WA5 7UN
England

Tel: +44 (0) 1925 445225
Fax: +44 (0) 1925 416518
Toll Free (USA): 1-888 96 HIDEN (44336)
E-mail: info@hiden.demon.co.uk
Web Site: http://www.HidenAnalytical.com

Appendix B: Atomic weights of common molecules

Name	Formula	Peak 1 m/e	Peak 1 %	Peak 2 m/e	Peak 2 %	Peak 3 m/e	Peak 3 %	rel sens
Acetone	C_3H_6O	43	100	58	33	15	20	3.6
Air		28	100	32	27	14	6	1.0
Ammonia	NH_3	17	100	16	80	15	8	1.3
Argon	Ar	40	100	20	16	36	0.3	1.2
Benzene	C_6H_6	78	100	77	19	52	16	5.9
Boron Trichloride	BCl_3	81	100	58	33	15	20	1.0
Carbon Dioxide	CO_2	44	100	16	9	14	6	1.4
Carbon Monoxide	CO	28	100	12	5	16	2	1.05
Carbon Tetrafluoride	CCl_4	69	100	50	12	19	7	1.0
Diborane	B_2H_6	26	100	27	97	24	90	1.0
Ethane	C_2H_6	28	100	27	33	30	26	2.6
Fomblin Oil		69	100	20	28	16	16	1.0
Freon 12	CCl_2F_2	85	100	87	32	50	16	2.7
Helium	He	4	100					0.14
Hydrogen	H_2	2	100	1	2			0.44

Name	Formula	Peak 1 m/e	Peak 1 %	Peak 2 m/e	Peak 2 %	Peak 3 m/e	Peak 3 %	rel sens
Hydrogen Chloride	HCl	36	100	38	32	35	17	1.6
Hydrogen Sulfide	H_2S	34	100	32	44	33	42	2.2
Krypton	Kr	84	100	86	31	82	21	1.7
Methane	CH_4	16	100	15	85	14	16	1.6
Methanol	CH_3OH	31	100	32	67	29	65	1.8
Neon	Ne	20	100	22	10	21	0.3	0.23
Nitrogen	N_2	28	100	14	5	29	1	1.0
Oxygen	O_2	32	100	16	9			0.86
Phosphine	PH_3	34	100	33	33	31	32	2.6
Pump Oil		57	100	55	73	43	73	1.0
Silane	SiH_4	30	100	31	78	29	29	1.0
Silicon Tetrafluoride	SiF_4	85	100	86	5	28	4	1.0
Sulfur Dioxide	SO_2	64	100	48	50	32	10	2.1
Water	H_2O	18	100	17	21	16	2	0.9
Xenon	Xe	132	100	129	98	131	79	3.0

Appendix C: Periodic Table